



High-fidelity Trotter formulas for digital quantum simulation

Yi-Xiang Liu (刘仪襄),^{1,2} Jordan Hines ,³ Zhi Li (李智),⁴ Ashok Ajoy,⁵ and Paola Cappellaro ^{1,2,6,*}

¹Research Laboratory of Electronics, Massachusetts Institute of Technology, Cambridge, Massachusetts 02139, USA

²Department of Nuclear Science and Engineering, Massachusetts Institute of Technology, Cambridge, Massachusetts 02139, USA

³Department of Physics, University of California Berkeley, Berkeley, California 94720, USA

⁴Department of Physics and Astronomy, University of Pittsburgh, and Pittsburgh Quantum Institute, Pittsburgh, Pennsylvania 15260, USA

⁵Department of Chemistry, University of California Berkeley, and Materials Science Division, Lawrence Berkeley National Laboratory, Berkeley, California 94720, USA

⁶Department of Physics, Massachusetts Institute of Technology, Cambridge, Massachusetts 02139, USA



(Received 11 November 2019; revised 6 April 2020; accepted 16 June 2020; published 14 July 2020)

Quantum simulation promises to address many challenges in fields ranging from quantum chemistry to material science and high-energy physics, and could be implemented in noisy intermediate-scale quantum devices. A challenge in building good digital quantum simulators is the fidelity of the engineered dynamics given a finite set of elementary operations. Here we present a framework for optimizing the order of operations based on a geometric picture, thus abstracting from the operation details and achieving computational efficiency. Based on this geometric framework, we provide two alternative second-order Trotter expansions: one with optimal fidelity at a short timescale, and the second robust at a long timescale. Thanks to the improved fidelity at different timescales, the two expansions we introduce can form the basis for experimental-constrained digital quantum simulation.

DOI: [10.1103/PhysRevA.102.010601](https://doi.org/10.1103/PhysRevA.102.010601)

Introduction. Simulation has been at the core of quantum information processing right from its inception, starting from Feynman's vision of simulating physics using a quantum system [1]. Quantum simulators are poised to be one of the first quantum devices to show task-specific quantum supremacy [2]. Quantum simulation has great potential impact on quantum chemistry [3–5], material science [6], condensed matter [7–10], and high-energy physics [11,12]. The most flexible strategy to achieve quantum simulation is via digital quantum simulation [13], where a target time-evolution operator is represented by a sequence of elementary quantum gates, usually involving one or two qubits. The strategy of approximating the continuous evolution with discrete gates is also known as Trotter expansion [14]. Finding a sequence of elementary operations that approximates a desired simulated Hamiltonian with high fidelity is crucial to practical implementations of digital quantum simulation. First- and second-order Trotter expansions with simple alternating patterns are most commonly used on experimental platforms, including superconducting qubits [3,8,9,15,16], trapped ions [7,17], atomic systems [18], and spin systems [10,19], although there has been a recent interest also in randomized Trotter expansions [20,21].

While the fidelity of digital quantum simulation can be increased by decreasing Trotter-step size, on all experimental platforms, the smallest Trotter step will eventually hit some practical limitations. In Hamiltonian simulation, the rotation angle under a specific Hamiltonian cannot be made arbitrarily small due to experimental constraints. For example, in a recent implementation of digital quantum simulation with trapped ions [7], the smallest flip angle of the unitary evolution block

was $Jt = \pi/16$, and similar numbers can be obtained in other experimental platforms [8,16]. Then, even the second-order Trotter sequence might not yield good enough fidelity. Higher-order expansions are usually hard to implement experimentally due to negative [22] coefficients, resulting in longer total evolution time. In many cases, it is desirable to engineer the simulated evolution from a finite set of elementary operations (gates). For example, in fault-tolerant quantum computation, the circuit is built up from a set of universal gates that can be implemented fault tolerantly [23,24].

In this Rapid Communication, we focus on finding second-order Trotter expansions that yield a better fidelity than the conventional second-order Trotter (2T) expansion [25,26], given the set of implementable gates. Finding the optimal sequence that yields the best fidelity requires integer optimization over the product of large operators describing the exact form of each gate, which can be computationally expensive. Here we present a geometric framework to optimize the sequence without calculating the quantum-mechanical propagators. Using this picture, we present two expansions: one minimizes the third-order Trotter error, and we call it 2-optimal (2O); the second one has better performance at a longer timescale, and we name it 2-diagonal (2D). Both methods have better fidelity than the 2T expansion and even third-order Trotter when the time step is larger.

Geometric method to calculate the Trotter error. We consider the problem of engineering a target operator $e^{-it \sum_L w_L H_L}$, which encapsulates a general quantum simulation task, using implementable gates $e^{-iH_k t/n}$. For illustration purposes let us first consider $L = 2$ and the target is e^{pA+qB} , where $A = -iH_1 t$ and $B = -iH_2 t$. Here we assume p and q to be integers and that the implementable gates are $e^{A/n}$ and $e^{B/n}$ (where $n > 0$

*pcappell@mit.edu

is also an integer). Under the constraints mentioned above, we can generally write any expansion as

$$e^{pa_1A/n} e^{qb_1B/n} \dots e^{pa_MA/n} e^{qb_MB/n} \approx e^{pA+qB}, \quad (1)$$

where $\sum_{k=1}^M a_k = \sum_{k=1}^M b_k = n$ and pa_k, qb_k are integers $\forall k$. The unitary fidelity F_U of expansion (1) up to $O(t^3)$ is

$$\begin{aligned} F_U &= e^{-(pA+qB)} (e^{pa_1A/n} e^{qb_1B/n} \dots e^{pa_MA/n} e^{qb_MB/n}) \\ &= \mathbb{1} + \mathcal{E}_2[A, B] + \mathcal{E}_{3,A}[A, [A, B]] + \mathcal{E}_{3,B}[B, [A, B]] + O(t^4) \end{aligned} \quad (2)$$

with

$$\mathcal{E}_2 = \frac{1}{2} \frac{pq}{n^2} \left(\sum_{k=1}^M b_k \sum_{m=1}^k a_m - \sum_{k=2}^M a_k \sum_{m=1}^{k-1} b_m \right), \quad (3)$$

$$\begin{aligned} \mathcal{E}_{3,A} &= \frac{1}{3n^3} \left[p^2 q \sum_{k=1}^M b_k \left(\sum_{m=1}^k a_m \right)^2 \right. \\ &\quad \left. - pq^2 \frac{1}{2} \sum_{k=2}^M a_k \left(\sum_{m=1}^{k-1} b_m \right) \left(2 \sum_{m=1}^k a_m - a_k \right) \right], \end{aligned} \quad (4)$$

and

$$\begin{aligned} \mathcal{E}_{3,B} &= \frac{1}{3n^3} \left[pq^2 \frac{1}{2} \sum_{k=1}^M b_k \left(\sum_{m=1}^k a_m \right) \left(2 \sum_{m=1}^k b_m - b_k \right) \right. \\ &\quad \left. - p^2 q \sum_{k=2}^M a_k \left(\sum_{m=1}^{k-1} b_m \right)^2 \right]. \end{aligned} \quad (5)$$

For example, the first-order Trotter expansion $(e^{pA/n} e^{qB/n})^n$ gives $F_U = \mathbb{1} + \frac{1}{2n} pq[A, B] + O(t^3)$. If p (or q) is even, we can engineer the 2T expansion,

$$(e^{pA/(2n)} e^{qB/n} e^{pA/(2n)})^n, \quad \text{with}$$

$$F_U = \mathbb{1} - \frac{1}{24n^2} pq(p[A, [A, B]] + 2q[B, [A, B]]) + O(t^4) \quad (6)$$

to achieve a better approximation (a similar expression holds for q even). There are complementary works [27–29] on optimizing expansion (1) to different orders for fixed M without the constraint that pa_k, qb_k are integers. However, the optimal expansions are not always implementable under the experimental limitations we are considering.

In general, finding the coefficients $\{pa_k, qb_k\}$ is a hard problem since it requires an integer optimization search performed by calculating F_U based on the exact form of the Hamiltonians $H_{1,2}$, which might be prohibitive when considering large quantum systems. Here we present a geometric method to approach this algebraic problem, which enables us to optimize the ordering without considering the exact forms of the Hamiltonians.

Any expansion in the form of Eq. (1), can be represented as a path on a grid picture, as shown in Fig. 1(a), giving the second-order and third-order Trotter errors geometric interpretation. The ideal operator e^{pA+qB} can be represented on the grid as a vector (np, nq) . One elementary gate is represented by a unit vector: $e^{A/n}$ is the unit vector $(1,0)$ and $e^{B/n}$ is the unit vector $(0,1)$. Starting from the origin $(0,0)$, at each

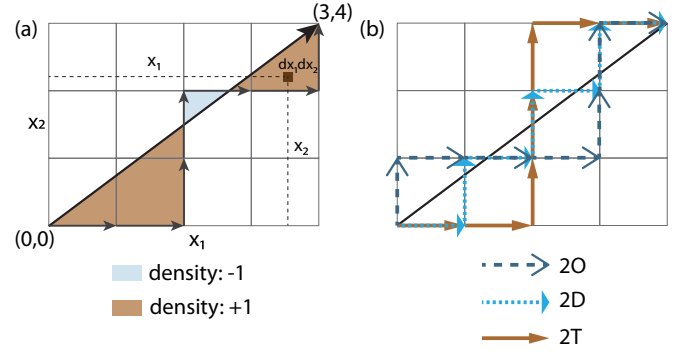


FIG. 1. Geometric method to calculate the Trotter error. (a) Geometric picture for Trotter expansion of e^{4A+3B} [vector $(4,3)$] by products of e^A 's and e^B 's. Unit vector $(1,0)$ represents e^A and unit vector $(0,1)$ represents e^B . Any path starting from $(0,0)$ that ends at $(4,3)$ is accurate to first order. The second-order error is the total area enclosed by the diagonal and the path, where any region below (above) the diagonal has an area density $+1$ (-1). The third-order error is given by the moments, where, e.g., the infinitesimal moment about x_2 axis is the area of the dark-brown square times the distance to the x_2 axis. (b) Examples of three different second-order paths. The dark-brown line is the conventional 2T expansion ($e^{2A} e^{3B} e^{2A}$). The dark-blue dashed path has a global minimum third-order error (2O, $e^B e^{3A} e^{2B} e^A$). The light-blue path has a minimal total distance from each node to the diagonal (2D, $e^A e^B e^A e^B e^A$), represented by the sum of absolute areas. All three paths enclose zero total area.

step we can move right (evolving under $e^{A/n}$) or up (evolving under $e^{B/n}$). A given ordering is then represented as a directed path on the grid. Figure 1(b) shows three different orderings for $p = 4$, $q = 3$, and $n = 1$. This grid representation can be regarded as a “projection” of the Trotterized process on the unitary group. More rigorously, the Trotterized unitary operators live in a fiber bundle, for which the grid is the base space (see Sec. I in [30] for details). On this grid picture, any path that ends at (np, nq) is accurate to first order. The second-order error of the path is given by [30]

$$\frac{1}{2} [A, B] \left(\oint_l x_1 dx_2 - x_2 dx_1 \right) = [A, B] \iint_D dx_1 dx_2, \quad (7)$$

where loop l is the Trotter path followed by vector $(-np, -nq)$, and D is the region enclosed by l . The coefficient of $[A, B]$ can be interpreted as the total area defined by the path and the diagonal: $\iint_D dx_1 dx_2$, where the areas below (above) the diagonal have density $+1$ (-1). Then, to cancel the second-order error, the area should sum up to zero. If we replace the discrete sum in Eq. (3) with an integral, we find $\mathcal{E}_2 = \frac{1}{2} \oint_l (x_1 dx_2 - x_2 dx_1)$, indicating that the brute-force calculation is consistent with the differential geometry calculation. The third-order error is [30]

$$\begin{aligned} &\frac{1}{3} [A, [A, B]] \oint_l x_1 (x_1 dx_2 - x_2 dx_1) \\ &+ \frac{1}{3} [B, [A, B]] \oint_l x_2 (x_1 dx_2 - x_2 dx_1) \\ &= [A, [A, B]] \iint_D x_1 dx_1 dx_2 + [B, [A, B]] \iint_D x_2 dx_1 dx_2. \end{aligned} \quad (8)$$

In the third-order error, the coefficient of $[A, [A, B]]$ ($[B, [A, B]]$) is the total moment about the x_2 axis (x_1 axis) defined by the path [see Fig. 1(a)]. Again, Eqs. (4) and (5) are discrete forms of the coefficients in Eq. (8). If all steps are restricted to be directional, that is, either along $(0,1)$ or $(1,0)$, the total moment is always nonzero, which is consistent with the *nonexistence theorem of positive decomposition* in [22]. In principle, a third-order expansion, which has zero total moments about both axes, can also be represented by this picture, by allowing walking left $(-1, 0)$ ($e^{-A/n}$) and down $(0, -1)$ ($e^{-B/n}$). This indeed leads, e.g., to the known third-order Trotter expansion known as Ruth's formula [31]. Given experimental constraints that typically do not allow simple inversion of the Hamiltonian arrow of time, we do not consider this scenario.

Using this geometric framework, we can now discuss two second-order sequences optimizing over different cost functions. The first sequence (2O) has a global minimum third-order error. The other sequence (2D) stays as close to the diagonal as possible and minimizes the distance from each node on the path to the diagonal. 2D has a better performance at a longer timescale, even if it is not optimal in terms of the third-order error. The algorithms used to find the two sequences have different computational complexities.

2-optimal sequence. In order to minimize the third-order error, we start by assigning each edge on the grid a triplet of weights given by Eq. (7) and the first line of Eq. (8). Using dynamic programming, we can find a path that puts the second-order error to zero and minimizes the third-order error. The main idea is that at each step, we keep track of the accumulated weights for each node, and finally select the path corresponding to the smallest absolute value weight. The details of the algorithm can be found in Sec. II in [30]. In general, the optimization should be done over all Trotter steps, thus on a grid $pn \times qn$. When the expansions become deep and optimizing over all Trotter steps is too expensive to calculate, one can optimize within a coprime (p, q) and repeat, or mirror symmetrize the smallest unit [32].

2-diagonal sequence. This algorithm is not based on the exact expression of the Trotter error, but rather on the intuition that being as close to the diagonal as possible should give a good approximation. There are different metrics to quantify “being close”; the 2D algorithm minimizes the distance from each node to the diagonal, thus minimizing the total distance, which can be shown to minimize the total unsigned area enclosed by the diagonal and the path as well. What is interesting is that the global distance optimal path can be found in a computationally efficient way by a greedy optimization (see Sec. III in [30] for the proof): at each step, we choose the move that ends closer to the diagonal. It can be shown that when p, q are mutually prime, and when at least one of them is even, 2D always finds a unique path, and the 2D path guarantees the second-order error to be zero. When both p and q are odd, 2D finds two opposite-order paths with opposite second-order error. We can then symmetrize the sequence to cancel the second-order error. That is, 2D can be made into a second-order expansion by optimizing and symmetrizing on the smallest unit grid $[2(p+q)$ steps], and the whole sequence is generated by repeating the smallest unit.

For some (p, q) 's, 2D and 2O share the same ordering, but in general, 2D does not have a global minimum third-order error. Still, we can prove that 2D still has smaller third-order error compared with the 2T expansion. The details of the proof can be found in Sec. IV of [30].

Both 2O and 2D can be easily generalized to higher dimension (see Fig. 2 in [30]), that is, to the scenario where we want to combine a larger number of propagators, $e^{A/n}$, $e^{B/n}$, $e^{C/n}$, etc. Figure 1(b) shows 2O, 2D, and 2T paths for $p = 4$, $q = 3$, and $n = 1$ on the grid picture. Figure 2(a) illustrates paths for $p = 12$, $q = 8$. Especially when higher dimensions are involved, the simpler greedy optimization of 2D is beneficial to reduce the computational complexity.

Numerical evaluations. When the Trotter-step size is small, 2O is optimal and 2D is better than 2T, regardless of the exact form of the Hamiltonian. Numerical calculation verifies both facts. Additionally, we found in numerical calculations over a variety of test Hamiltonians that 2D is better than 2T at longer times. In the following numerical calculations, we only compare expansions up to $p+q = 20$. Though the dynamic programming time and space complexities are polynomial in the grid dimension, the computation for 2O quickly becomes both time-consuming and space-consuming as p and q become larger.

The metric we use to quantify the performance is the average fidelity of a quantum gate [33], which reads

$$F = |\text{Tr}(U_1^\dagger U_2)| / \text{Tr}(U_1^\dagger U_1), \quad (9)$$

where U_1 is the ideal operator and U_2 is the approximated one. To further highlight differences in fidelity, we plot the log fidelity $F_l = -\log_{10}(1 - F)$. We also considered $\|U_1 - U_2\|$, where $\|\cdot\|$ is Frobenius norm, as a metric of error, and the results are qualitatively the same.

The orderings of the three second-order Trotter expansions for $p=12$, $q=8$ are shown in Fig. 2(a). Figure 2(b) shows the numerical results for a two-spin transverse-field Ising Hamiltonian, $H = 12H_1 + 8H_2$, where $H_1 = \frac{1}{2}(\sigma_z^1 + \sigma_z^2)$ and $H_2 = \sigma_x^1 \sigma_x^2$. Then $A = -iH_1 t$, $B = -iH_2 t$. For different (p, q) pairs (here with $p+q = 20$) the results look qualitatively the same. We also verified that the same qualitative results apply for different Hamiltonians and different system sizes, such as a transverse-field Ising model with next-nearest-neighbor coupling for two to ten spins, and an alternating dipolar model with three to eight spins (see Sec. V in [30]).

We can first verify that all three expansions are second-order expansions with respect to t by fitting the data to $F_l = -a \log_{10} t + b$ and extract the slope a at small t [see the solid lines in Fig. 2(b)]. From the Taylor expansion we expect $a = 6$ and the fitted values for 2O, 2D, and 2T are 6.07, 5.99, and 5.99, respectively. In the short t regime, 2O shows the best fidelity, as expected since it minimizes the third-order error. 2D also provides a higher fidelity than the conventional 2T expansion for all t . At some t , 2D even starts to outperform 2O, the crossover point being around $t \|H_1\| = 0.14$. Figure 2(c) shows a histogram of crossover point positions over 1000 pairs of random Hermitian matrices $H_{1,2}$. The center of the Gaussian depends highly on specific (p, q) , but it is always on the order of 0.1. For typical experimental values,

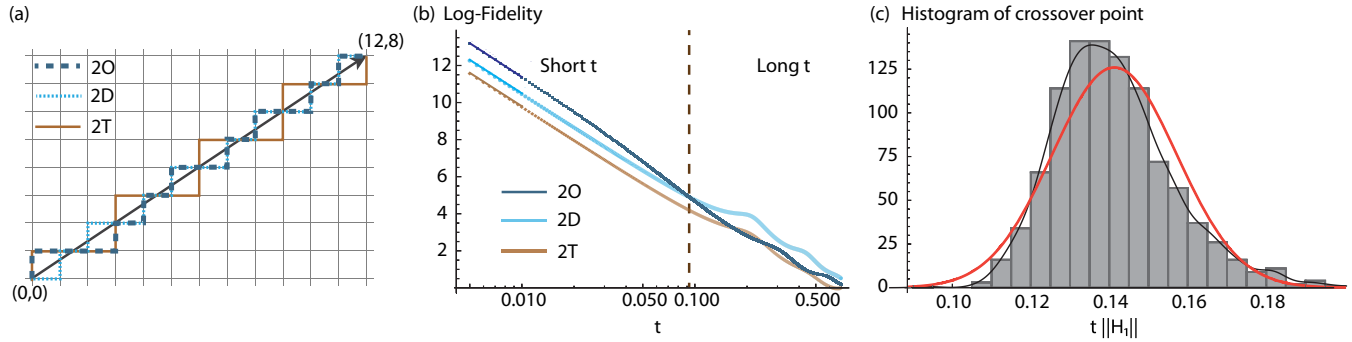


FIG. 2. Fidelity comparison for the three Trotter sequences. (a) Geometric illustration of three different second-order approximations to e^{12A+8B} . In (a) and (b) dark-blue lines are for the 2O path, light-blue for 2D, and brown for 2T. (b) Numerical evaluation of log fidelity. Here $A = -iH_1t/n$, $B = -iH_2t/n$, where $H_1 = \frac{1}{2}(\sigma_z^1 + \sigma_z^2)$, $H_2 = \sigma_x^1\sigma_x^2$, and $n = 1$. At short t , 2O shows the best fidelity since it has the smallest third-order error. At very small t we fit the simulated data to $F_t = -\log_{10}(1 - F) = -a \log_{10} t + b$, and the slopes of 2O, 2D, and 2T are 6.07, 5.99, and 5.99, respectively, close to the expected result, 6, for second-order expansions. 2D starts to outperform 2O around $t = 0.13/\|H_1\|$, where $\|\cdot\|$ is the Frobenius norm. Going beyond the time of the simulation, it is possible that 2O outperforms 2D again. However, at these long times the fidelity is low and not useful for quantum simulations. (c) Histogram of crossover point (where 2O and 2D intersect) for 1000 pairs of random 4×4 Hermitian matrices $H_{1,2}$. The black solid curve is the smoothed histogram and the orange curve is a Gaussian fit to the histogram. The mean and variance of the Gaussian distribution are 0.14 and 0.02, respectively.

such as $Jt = \pi/16$ [7] and $U\Delta t/2 = 5/16$ [16], 2D is then the best sequence. We can explain this result by noting, as described in detail in [30], that the error of an arbitrary path is always bounded by the total unsigned area. Since this is a non-perturbative result, it suggests that a path with minimal total unsigned area, which is equivalent to 2D, will typically have better fidelity when the small-step expansion breaks down.

Conversely, these results imply that 2D does not need as small a Trotter step to reach the same fidelity. Then, the number of elementary gates needed to reach a given fidelity is smaller, a practical advantage for digital simulation [21], especially when fault-tolerant gates are required. We further evaluated the 2D performance with respect not only to the time step but also to the number of “switching” operations needed, finding that 2D performs well even under this metric (see Sec. VII in [30]). We also compared 2D and 2T assuming that the time-step resolution in 2T is not limited, and found that the performance of 2D is still comparable to 2T even though this condition is in favor of 2T (see Sec. VIII in [30]). We further find that 2D can outperform the third-order Trotter expansion, and the simplest sequence achieved by building an approximated 2T form with the smallest possible step, and then adding a naive alternation to reach the desired p, q (see Sec. IX in [30]).

Conclusions and outlook. Finding the exact global optimal Trotter sequence or even just the sequence minimizing the minimal third-order error can be expensive to calculate. In this Rapid Communication, we introduced two Trotter sequences

to achieve higher fidelity in digital quantum simulation, by exploiting a geometric framework to estimate the Trotterization error. By optimization of the fidelity on a simple grid picture, our 2O and 2D sequences outperform the widely used 2T sequence in complementary Trotter-step regimes. In addition, the 2D solution is based on an intuitive ordering that can be found with an efficient, greedy optimization algorithm. Compared to 2T, less Trotter steps are required to reach the same fidelity with our sequences, thus also providing an advantage when the Trotter-steps number is a performance metric.

We note that while we mostly presented numerical results for two qubits, we numerically obtain similar performances for larger systems, and indeed the scalings found are expected to apply to many-qubit systems. As the minimization algorithm is very efficient, since it does not require one to evaluate quantum propagators, and it can be easily extended to deal with multiple building block operators, 2O and 2D can become versatile and powerful tools to improve the fidelity of digital quantum simulation for many-qubit systems. It could be interesting to further investigate applying our 2D and 2O sequences to other quantum algorithms beyond quantum simulation, such as quantum phase estimation [21,34] or to find a good ansatz for the quantum approximate optimization algorithm [35].

Acknowledgments. We thank Chao Yin (尹超) for helpful discussions. This work was supported in part by DARPA D18AC00024, NSF Grants No. EECS1702716 and No. PHY1734011.

[1] R. P. Feynman, *Int. J. Theor. Phys.* **21**, 467 (1982).

[2] J. Preskill, [arXiv:1203.5813](https://arxiv.org/abs/1203.5813).

[3] P. J. J. O’Malley, R. Babbush, I. D. Kivlichan, J. Romero, J. R. McClean, R. Barends, J. Kelly, P. Roushan, A. Tranter, N. Ding *et al.*, *Phys. Rev. X* **6**, 031007 (2016).

[4] A. Aspuru-Guzik, A. D. Dutoi, P. J. Love, and M. Head-Gordon, *Science* **309**, 1704 (2005).

[5] C. Hempel, C. Maier, J. Romero, J. McClean, T. Monz, H. Shen, P. Jurcevic, B. P. Lanyon, P. Love, R. Babbush *et al.*, *Phys. Rev. X* **8**, 031022 (2018).

- [6] R. Babbush, N. Wiebe, J. McClean, J. McClain, H. Neven, and Garnet Kin-Lic Chan, *Phys. Rev. X* **8**, 011044 (2018).
- [7] B. P. Lanyon, C. Hempel, D. Nigg, M. Müller, R. Gerritsma, F. Zähringer, P. Schindler, J. T. Barreiro, M. Rambach, G. Kirchmair *et al.*, *Science* **334**, 57 (2011).
- [8] Y. Salathé, M. Mondal, M. Oppliger, J. Heinsoo, P. Kurpiers, A. Potočnik, A. Mezzacapo, U. Las Heras, L. Lamata, E. Solano *et al.*, *Phys. Rev. X* **5**, 021027 (2015).
- [9] N. K. Langford, R. Sagastizabal, M. Kounalakis, C. Dickel, A. Bruno, F. Luthi, D. J. Thoen, A. Endo, and L. DiCarlo, *Nat. Commun.* **8**, 1715 (2017).
- [10] K. X. Wei, C. Ramanathan, and P. Cappellaro, *Phys. Rev. Lett.* **120**, 070501 (2018).
- [11] E. A. Martinez, C. A. Muschik, P. Schindler, D. Nigg, A. Erhard, M. Heyl, P. Hauke, M. Dalmonte, T. Monz, P. Zoller, and R. Blatt, *Nature (London)* **534**, 516 (2016).
- [12] E. Zohar, J. I. Cirac, and B. Reznik, *Rep. Prog. Phys.* **79**, 014401 (2016).
- [13] S. Lloyd, *Science* **273**, 1073 (1996).
- [14] H. F. Trotter, *Proc. Am. Math. Soc.* **10**, 545 (1959).
- [15] L. Lamata, A. Parra-Rodriguez, M. Sanz, and E. Solano, *Adv. Phys.: X* **3**, 1457981 (2018).
- [16] R. Barends, L. Lamata, J. Kelly, L. García-Álvarez, A. G. Fowler, A. Megrant, E. Jeffrey, T. C. White, D. Sank, J. Y. Mutus *et al.*, *Nat. Commun.* **6**, 7654 (2015).
- [17] I. Arrazola, J. S. Pedernales, L. Lamata, and E. Solano, *Sci. Rep.* **6**, 30534 (2016).
- [18] H. Weimer, M. Müller, I. Lesanovsky, P. Zoller, and H. P. Büchler, *Nat. Phys.* **6**, 382 (2010).
- [19] A. Ajoy and P. Cappellaro, *Phys. Rev. Lett.* **110**, 220503 (2013).
- [20] A. M. Childs, A. Ostrander, and Y. Su, *Quantum* **3**, 182 (2019).
- [21] E. Campbell, *Phys. Rev. Lett.* **123**, 070503 (2019).
- [22] M. Suzuki, *J. Math. Phys.* **32**, 400 (1991).
- [23] M. A. Nielsen and I. L. Chuang, *Quantum Computation and Quantum Information* (Cambridge University Press, Cambridge, New York, 2000).
- [24] N. C. Jones, J. D. Whitfield, P. L. McMahon, M.-H. Yung, R. V. Meter, A. Aspuru-Guzik, and Y. Yamamoto, *New J. Phys.* **14**, 115023 (2012).
- [25] M. Suzuki, *J. Stat. Phys.* **43**, 883 (1986).
- [26] M. Suzuki, *Phys. Lett. A* **146**, 319 (1990).
- [27] T. Barthel and Y. Zhang, *Ann. Phys.* **418**, 168165 (2020).
- [28] R. I. McLachlan, *SIAM J. Sci. Comput.* **16**, 151 (1995).
- [29] B. D. M. Jones, D. R. White, G. O. O'Brien, J. A. Clark, and E. T. Campbell, in *Proceedings of the Genetic and Evolutionary Computation Conference (GECCO '19)* (ACM, New York, 2019), pp. 1223–1231.
- [30] See Supplemental Material at <http://link.aps.org/supplemental/10.1103/PhysRevA.102.010601> for details of the geometrical framework, algorithm for 2-optimal, analytical bounds on 2-diagonal fidelity, and more numerical examples, which includes Refs. [8,10,22,24,31,36–44].
- [31] R. D. Ruth, *IEEE Trans. Nucl. Sci.* **30**, 2669 (1983).
- [32] When both p and q are odd, it is not possible to cancel the second-order error and one needs to perform the optimization on a $(2p, 2q)$ unit grid.
- [33] M. A. Nielsen, *Phys. Lett. A* **303**, 249 (2002).
- [34] D. S. Abrams and S. Lloyd, *Phys. Rev. Lett.* **83**, 5162 (1999).
- [35] E. Farhi, J. Goldstone, and S. Gutmann, [arXiv:1411.4028](https://arxiv.org/abs/1411.4028).
- [36] S. Kobayashi and K. Nomizu, *Foundations of Differential Geometry*, A Wiley Publication in Applied Statistics Vol. 1 (Wiley, New York, 1996).
- [37] G. Erlend and P. Pierre, *Forum Math.* **30**, 1363 (2018).
- [38] C. H. Taubes, *Differential Geometry: Bundles, Connections, Metrics and Curvature* (Oxford University Press, New York, 2011).
- [39] U. Schreiber and K. Waldorf, *Homology, Homotopy Appl.* **13**, 143 (2011).
- [40] P. Peng, C. Yin, X. Huang, C. Ramanathan, and P. Cappellaro, [arXiv:1912.05799](https://arxiv.org/abs/1912.05799).
- [41] M. H. Abobeih, J. Cramer, M. A. Bakker, N. Kalb, M. Markham, D. J. Twitchen, and T. H. Taminiau, *Nat. Commun.* **9**, 2552 (2018).
- [42] N. Bar-Gill, L. Pham, A. Jarmola, D. Budker, and R. Walsworth, *Nat. Commun.* **4**, 1743 (2013).
- [43] G. A. Álvarez, D. Suter, and R. Kaiser, *Science* **349**, 846 (2015).
- [44] J. Zhang, P. W. Hess, A. Kyprianidis, P. Becker, A. Lee, J. Smith, G. Pagano, I.-D. Potirniche, A. C. Potter, A. Vishwanath, N. Y. Yao, and C. Monroe, *Nature (London)* **543**, 217 (2017).